Bioactive Materials 51 (2025) 383–398

Contents lists available at ScienceDirect

Bioactive Materials

journal homepage: www.keaipublishing.com/en/journals/bioactive-materials

Pretreated exosomes by electrical stimulation accelerate bone regeneration

Jialu Chen [a,b,1], Jian Chen [c,1], Jiahao Chen [a,b,1], Renjie Lu [a,b], Ziyuan Liu [b], Yang Zhang [b,d,*], Chi Zhang [c,**]

[a] Department of Orthopedics, Shanghai Sixth People's Hospital Affiliated to Shanghai Jiao Tong University School of Medicine, Shanghai, 200236, China
[b] Nanomedicine and Intestinal Microecology Research Center, Shanghai Tenth People's Hospital, School of Medicine, Tongji University, Shanghai, China
[c] Department of Orthopedics, Shanghai General Hospital, Shanghai Jiao Tong University School of Medicine, Shanghai Jiao Tong University, Shanghai, 200080, China
[d] Department of Pharmacy, Shanghai Eighth People's Hospital, School of Medicine, Tongji University, Shanghai, China

ARTICLE INFO

Keywords:
Electrical stimulation
Pretreated
Exosome
Bone regeneration
Bone tissue engineering

ABSTRACT

Bone tissue engineering has attracted significant attention from both the research and clinical communities. Inspired by the inherent bioelectric properties of bone tissue, electrical stimulation is widely recognized as an external intervention that can induce osteogenesis, mineralization, and accelerate bone regeneration. However, the clinical application of electrical stimulation is limited by the complexity of the procedures and the use of cumbersome, invasive equipment. Exosomes, as an alternative to seed cells, can overcome many of the limitations associated with stem cell transplantation. Researchers aim to enhance exosomes' therapeutic potential for bone regeneration. While various pretreatments have been studied, there is currently no research investigating the role of exosomes pretreated with electrical stimulation in bone tissue regeneration. In this study, we pretreated bone marrow mesenchymal stem cells (BMSCs) with electrical stimulation and isolated the resulting exosomes (Elec-exo). A series of in vitro experiments determined that 150 μA is the optimal condition for electrical stimulation. Mechanistically, proteomic analysis revealed an enrichment of proteins involved in "Oxidative Phosphorylation" regulation within Elec-exo, and transcriptomic analysis indicated the activation of Pl3k-Akt and MAPK bone formation-related signaling pathways in the effector cells. Hydrogels, as a sustained-release scaffold, were used to deliver Elec-exo in vivo. In a rat femur defect model, Elec-exo loaded into chondroitin sulfate methacrylate (CSMA) hydrogel accelerated early bone tissue regeneration. In summary, our study explores the mechanisms by which electrical stimulation pretreatment enhances bone tissue regeneration and broadens the therapeutic application of exosomes in accelerating bone regeneration.

1. Introduction

Bone defects (BDs) caused by traumatic injuries, osteoporosis or tumor excision represent a challenging problem in public health [1][2]. Postoperative rehabilitation problems include prolonged hospital stay, increased postoperative complications and treatment costs, which bring a considerable burden to patients. Autografts, allografts and xenograft have been relatively successful as clinical therapeutic strategies for repairing critical-sized bone defects. Despite their limitations, such as the limited source of donors, immune response, inferior healing and the possibility of infection following surgery [][3]. Recently, bone tissue engineering, including scaffolds, cells and growth factors, has been considered as a promising approach offers a promising approach to expedite bone repair or regeneration and overcome these limitations [4].

Bone is considered as an electroactive and electrosensitive tissue with piezoelectric, pyroelectric, ferroelectric and other characteristics [4]. It has been reported that the physiological potential ranges from −60 to −100 mV [5]. The bone defect area typically lacks an endogenous electric field, which results in the disruption of the

Peer review under the responsibility of editorial board of Bioactive Materials.
* Corresponding author. Department of Pharmacy, Shanghai Eighth People's Hospital, School of Medicine, Tongji University, Shanghai, China;8 Caobao Road, Shanghai, 200235, China.
** Corresponding author. Department of Orthopedics, Shanghai General Hospital, Shanghai Jiao Tong University School of Medicine, Shanghai Jiao Tong University, 100 Haining Street, Shanghai, 200080, China.
E-mail addresses: zhangyang0202@tongji.edu.cn (Y. Zhang), hydraliskrush@sjtu.edu.cn (C. Zhang).
[1] These authors contributed equally to this work.

https://doi.org/10.1016/j.bioactmat.2025.04.019
Received 13 January 2025; Received in revised form 27 March 2025; Accepted 16 April 2025

microenvironment. The restoration of the local bioelectrical microenvironment is integral to the entire process of bone defect regeneration. In the absence of local bioelectrical stimulation, the migration of osteoblasts from the edges to the center of the defect area is also a time-consuming endeavor [6]. Since Fukada et al. described the positive osteogenic effect of electrical stimulation (ES) in fracture healing, electrical stimulation has attracted much attention as an important biophysical stimulation and non-drug intervention [7–9]. However, the current widespread use of ES therapy is also limited by cumbersome external equipment and complex operation management.

Bone marrow-derived mesenchymal stem cells (BMSCs) have been shown to be beneficial for bone tissue regeneration. Recent studies have shown that BMSCs play a therapeutic and regulatory role mainly through the paracrine pathway [10–13]. Exosome are important carriers of intercellular communication, transporting proteins, lipids and RNA, and regulating cell function [14,15]. Exosomes are a type of extracellular vesicles, measuring 30–200 nm in diameter [16], that are secreted from cells through the multivesicular endosomal pathway [17,18].

Over the past decade, studies have focused on engineering exosome to improve the bioactivity, stability, and biological functions of native exosome [19–21]. Several approaches, such as genetic manipulation and chemical surface modification, have been proposed to engineer exosome. However, these approaches are technically complex. Cultivating parental cells in a conditioned medium that simulates the healing microenvironment, such as hypoxia [22–25], addition of bioactive molecules [26–28], three-dimensional culture [29], and magnetic field stimulation [30], provides a simple and effective method for exosome engineering. What's more, electrical stimulation is also a good stimulation for bone tissue engineering [31–33]. Electroconductive substrate-mediated electrical stimulation is a classic method for in vitro cell electrical stimulation. Electroconductive substrate-mediated electrical stimulation is a classic method for in vitro cell electrical stimulation. This method constructs a cell culture substrate using conductive materials (such as carbon-based materials, indium tin oxide (ITO), conductive polymers, etc.) and achieves cell stimulation by applying a controllable current to the substrate. The conductive substrate serves not only as a biological interface for cell attachment but also as a physical medium for the transmission of the electric field. It can provide a uniform electric field, stable and controllable electrical stimulation, and can be customized into various shapes and sizes, thereby establishing a biomimetic electrophysiological regulation system in the cell microenvironment.

To overcome the technical bottlenecks in the isolation, loading, and release of exosomes, hydrogels have emerged as an ideal material for exosome delivery, thanks to their excellent biocompatibility and tunable physicochemical properties.

Chondroitin sulfate (CS) is a negatively charged glycosaminoglycan found in the non-collagenous extracellular matrix (ECM) of bone tissues [34,35]. Chondroitin sulfate methacrylate (CSMA) is a photo-crosslinked hydrogel based on chondroitin sulfate [36]. Due to its excellent injectability and osteoinductive capabilities, it can play a variety of roles in bone tissue engineering. [37,38]. Studies have shown that chondroitin sulfate can promote bone regeneration [39]. CSMA has good biocompatibility and can exert the physiological activity of chondroitin sulfate to promote bone regeneration and accelerate the healing of bone defects [39].

Therefore, our experimental design is to extract and collect exosomes secreted by cells after normal culture and electrical stimulation, and use chondroitin sulfate hydrogel to encapsulate the load to construct an injectable hydrogel of electrical stimulation functionalized exosomes.

2. Material and methods

2.1. Isolation and culture of rat bone marrow mesenchymal stem cells (RBMSCs) and rat osteoblasts (ROBs)

To isolate bone marrow mesenchymal stem cells (BMSCs) [41], six-week-old SD rats were anesthetized with 2 % sodium pentobarbital and then soaked in 75 % alcohol for 10 min for disinfection. Subsequently, the femurs were isolated and the bone marrow cavity was flushed with cell culture medium. The collected bone marrow flush was filtered through a mesh screen and then centrifuged at 1000 g for 3 min. Finally, the pellet was resuspended and seeded into a 10 cm culture dish.

To obtain osteoblasts (ROBs), the calvarial bones from neonatal SD rats were used [41]. The calvarial tissues were minced and sequentially digested with 1 % trypsin for 10 min and then centrifuged at 1000 g for 3 min. The supernatant was discarded, and the remaining tissue was digested with 0.2 % type I collagenase (Gibco, USA). The digested calvarial fragments were resuspended in cell culture medium and cultured in a 37 °C, 5 % CO_2 incubator.

Both the obtained BMSCs and ROBs were cultured in α-MEM medium supplemented with 10 % fetal bovine serum (FBS) and 1 % penicillin/streptomycin (PS), with the medium being changed every 3 days. When the cell confluence reached 80 %–90 %, the cells were passaged.

2.2. Electrical stimulation of bone marrow mesenchymal stem cells

A 15 cm cell culture dish was selected, and a circular ITO conductive glass with a diameter of 135 mm was custom-made according to its size parameters (the resistance of the glass was previously determined to be less than 10 Ω). The conductive glass was connected in series to a BLU939 power analyzer via terminals and wires, and the accompanying software was launched. Based on the recommended electrical stimulation intensities from the literature, the cells were divided into three groups with different electrical stimulation strengths: 20 μA, 75 μA, and 150 μA. The parameters were adjusted according to the selected current levels for stimulation, with a frequency of 1 h per day for 5 consecutive days. BMSCs pre-treated with electrical stimulation (Elec-BMSCs) were ultimately obtained.

2.3. Isolation of normal exosomes (Norm-exo) and exosomes from electrical stimulated BMSCs (Elec-exo)

Cell culture: Elec-BMSCs and Norm-BMSCs (BMSCs without electrical stimulation pre-treatment) were cultured in MEM-α medium.

Collect electrical stimulation pretreatment and normal mesenchymal cell exosomes:

The electrical stimulation pretreatment and normal mesenchymal cells were expanded to 10 dishes in the form of cell passage. When the fusion rate reached 70 %–80 %, MEM-α complete medium was removed. The cells were gently rinsed with phosphate buffered saline (PBS) repeatedly, and the residual liquid was sucked out and replaced with MEM-α basal medium. The supernatant was collected after 24 h of culture. After collecting a sufficient amount of supernatant, continuous low-temperature centrifugation was performed in a low-temperature centrifuge at 4 °C, with a parameter of 300 g, 10 min; 3000 g, 10 min and 10000 g, 30 min. After each centrifugation, carefully transfer the supernatant to a new centrifuge tube and then proceed to the next centrifugation. In an ultracentrifuge, centrifuge at 125,000 g for 75 min. Remove the supernatant and rinse the tube wall with 100 μL of PBS to obtain a concentrated crude exosome product. To obtain PKH26-stained exosomes, add 10 μL of 2×10^{-5} M PKH26 dye solution to the collected crude exosome product, mix by vertexing for 1 min, and let it stand for 10 min. Then, add 1 mL of PBS containing 10 % exosome-depleted serum to stop the staining. Rebalance the tubes and continue centrifugation in the ultracentrifuge at 125,000 g for 75 min. Depending on the electrical stimulation pretreatment intensity of the donor cells, collect

the final exosomes and label them as Norm-exo and Elec-exo (20 μA-exo, 75 μA-exo, and 150 μA-exo).

2.4. Characterization of Norm-exo and Elec-exo

The size distribution and concentration of Norm-exo and Elec-exo were determined using nanoparticle tracking analysis (NTA) and dynamic light scattering (DLS) analyzer. Also, the morphology of Norm-exo and Elec-exo was visualized using cryogenic transmission electron microscope (HITACHI H-7650).

2.5. Western blot assay

Briefly, exosomes or cells were lysed with RIPA buffer containing 1 % PMSF on ice for 30 min. The protein samples were collected and centrifuged at 12500 rpm for 5 min at 4 °C. Protein concentrations from each group were determined using the BCA method. Equal amounts of protein were then mixed with Loading Buffer and loaded onto an SDS-PAGE gel for electrophoresis. The proteins were transferred to a membrane, which was cut and blocked before incubating overnight with primary antibodies against CD9, CD63, Alix, Calnexin Akt, p-Akt and GAPDH. Secondary antibodies were used to detect the bound primary antibodies. Finally, the proteins were visualized using an ECL chemiluminescent substrate.

2.6. Quantitative real-time PCR (qRT-PCR)

BMSCs and osteoblasts were cultured in a CO2 incubator. When the cells were in good condition, they were placed into a 6-well plate and divided into 5 groups, with 3 wells per group and a density of $2*10^5$/holes. When the fusion rate reached 60 %, PBS (Group Control) or the PBS solution containing 40 μg of Norm-exo (Group 0), 20 μA-exo (Group 20), 75 μA-exo (Group 75), or 150 μA-exo (Group 150) protein was added to each group of wells. MEM-α complete medium was then added to each well to a total volume of 2 mL, and the cells were incubated in the incubator for a co-culture of 48 h. Total RNA was extracted from each group using TRIzol, and the RNA concentration was measured using a NanoDrop. The TAKARA PrimeScript™ RT reagent kit (TAKARA, Japan) was used to reverse transcribe 1000 ng of RNA into cDNA. The Taq Pro Universal SYBR qPCR Master Mix (Vazyme, China) was utilized to construct the qRT-PCR system, and the LightCycler® RealTime PCR 96 Systems were employed to detect the expression of osteogenic marker genes (BMP, OCN, and Col1A1) in the ROBs and RBMSCs of each group. The relative mRNA expression levels for each target gene were calculated using the $2^{-\Delta\Delta Ct}$ method, with the expression level of β-actin serving as the internal reference.

2.7. Alkaline phosphatase and alizarin Red S staining

After 7 days of treatment, ROBs were stained for alkaline phosphatase (ALP) using the BCIP/NBT Alkaline Phosphatase Color Development Kit (Beyotime, China). In the cell culture hood, the culture medium was removed, and ROBs were gently washed 5 times with PBS. The cells were then fixed with 4 % paraformaldehyde for 3 min, followed by washing with washing buffer (PBS containing 0.05 % v/v Tween 20). After the final wash, the washing buffer was removed, and an appropriate amount of BCIP/NBT staining working solution was added to cover the cell monolayer. The cells were incubated at room temperature in the dark for 25 min. Following incubation, the staining solution was carefully removed, and the cells were rinsed with distilled water. The stained cells were observed under a microscope, and images were captured for further analysis.

After 21 days of treatment, ROBs were stained for osteogenesis using the Osteogenesis Assay Kit (Beyotime, China). The cells were washed with PBS and fixed with the provided fixing solution for 20 min. The fixed cells were then rinsed with PBS to remove any residual fixing solution, and an appropriate amount of Alizarin Red S staining solution was added. The cells were stained at room temperature in the dark for 30 min, followed by thorough rinsing with distilled water. The stained cells were observed and photographed under a microscope. Finally, the integrated density values of the images from each group were quantitatively analyzed using ImageJ software.

2.8. Cell proliferation experiment

The proliferation of RBMSCs and ROBs after exosomes treatment was assessed by the CCK-8 assay. The cells were spread into 96-well plates and divided into 5 groups, 5 wells in each group, with a density of 5000 cells/well. When the fusion rate reached about 60 %, the Norm-exo, 20 μA-exo, 75 μA-exo and 150 μA-exo exosome solutions containing 1 μg protein were added to each group of wells, and the MEM-α complete medium was supplemented to 100 μL per well. The cells were incubated in a cell incubator for 24 h. The OD value of each group was detected by CCK-8 method, and the cell proliferation ability of each group was calculated.

2.9. Synthesis of CSMA hydrogel

CSMA is purchased from "ENGINEERING FOR LIFE" company. To explore how different hydrogel concentrations affect bone regeneration, we formulated hydrogels at three distinct concentrations: 4 %, 7 %, and 10 %, with PBS serving as the control group.

To prepare the 0.25 % (w/v) initiator stock solution, 10 mL of PBS was added to a brown bottle containing 0.025 g of lithium phenyl-2,4,6-trimethylbenzoylphosphinate (LAP). The mixture was heated in a water bath at 40–50 °C for 15 min with intermittent shaking to ensure complete dissolution. For the preparation of the CSMA solution (recommended concentration: 4–10 % w/v), CSMA was weighed at 0.04 g, 0.07 g, and 0.1 g, corresponding to the desired mass fractions, and transferred into separate centrifuge tubes. Subsequently, 1 mL of the initiator stock solution was added to each tube. The mixtures were dissolved at room temperature in the dark for 30 min with occasional shaking. Finally, the CSMA solutions were sterilized by passing through a 0.22 μm sterile syringe filter and stored in the dark for further use. To induce gelation of the CSMA solution, a UV lamp with a wavelength of 405 nm was used as the light source. The solution was irradiated for 45 s to initiate the gelation process.

2.10. Loading of exosomes into CSMA hydrogel

To prepare exosome-loaded CSMA hydrogels, Norm-exo and Elec-exo were uniformly diluted to 400 μg/mL using PBS. Subsequently, 500 μL of the exosome solution was mixed with 500 μL of 0.5 % (w/v) initiator solution at 4 °C under gentle vertexing to form an exosome-containing initiator solution. The subsequent steps for fabricating exosome-encapsulated CSMA hydrogels followed the same synthesis protocol as described above for hydrogel preparation. Thus, the exosome concentration in our in vivo hydrogel-exo system was standardized to 200 μg/mL.

For in vitro experiments, a UV lamp with a wavelength of 405 nm was used as the light source for 30 s of irradiation. The mixed solution was extruded at a constant rate from a syringe and allowed to stand briefly to obtain exosome-loaded CSMA hydrogels.

2.11. In vitro and In vivo release of exosomes in CSMA hydrogel

To evaluate the in vitro release of exosomes, three replicates in a 96-well plate were each injected with 50 μL of CSMA solution containing exosomes. The solution was then exposed to UV light for 30 s to induce gelation. Subsequently, 50 μL of PBS was added to each well, and the plate was incubated in a CO_2 incubator. At predetermined time points (Days 1, 2, 3, 4, 5, 7, 9, 11, and 14), 50 μL of the PBS supernatant was

carefully aspirated from each well and transferred to a new 96-well plate. The protein concentration in the collected supernatant was measured using a NanoDrop spectrophotometer. The data were processed to determine the amount and percentage of exosome release from CSMA over this period. After each sampling, the wells were gently washed several times with PBS, and any residual liquid was carefully removed using a pipette. Fresh 50 μL of PBS was then added to each well for the next time point analysis.

To evaluate the in vivo release of exosomes, 50 μL of CSMA hydrogel containing PKH26-labeled exosomes was injected into the distal femur of mice. At predetermined time points (Days 1, 5, 10, and 15), in vivo fluorescence distribution images were captured using a small-animal imaging system (BLT AV100).

2.12. Cell transcriptomics, Exosome proteomics, and Result analysis

For cell transcriptomics, The BMSC cells were divided into four groups: Control group: no treatment was applied; Elec-stimulated group: BMSC cells subjected to electrical stimulation at 150 μA for 1 h per day for a total of 5 days; Norm-exo group: BMSC cells co-incubated with exosomes derived from Norm-BMSCs for 2 days; Elec-exo group: BMSC cells co-incubated with exosomes derived from Elec-BMSCs for 2 days. Total RNA was extracted from each group of cells using the Trizol method. The RNA concentration and A260/A280 ratio were measured using NanoDrop to assess RNA purity and quality. Library construction was performed by APExBIO, and sequencing was conducted on the Illumina NovaSeq 6000 platform. Post-sequencing, data quality was verified using FastQC. Gene expression levels were quantified, and differential expression analysis was carried out. Functional annotations and enrichment analyses were performed, and results were visualized using ggplot2.

For exosome proteomics, exosomes were divided into two groups: Norm-exo group (exosomes derived from Norm-BMSCs) and Elec-exo group (exosomes derived from Elec-BMSCs). Exosome proteins were extracted using a method akin to Western Blot procedures. Peptide separation, mass spectrometry analysis, and subsequent proteomics quantitative analysis and functional annotation were all performed by APExBIO company.

2.13. Establishment of rat femoral defect model and Grouping

To mitigate the effects of estrogen, we selected 6-week-old Sprague-Dawley (SD) rats and administered anesthesia via intraperitoneal injection of sodium pentobarbital. The fur surrounding the target knee joint was carefully removed, and an incision was made through the skin using a scalpel. Utilizing hemostatic forceps and scissors, we meticulously separated the underlying tissues to expose the periosteum of the distal femur. Subsequently, employing an orthopedic drill and Kirschner wire, we created a cylindrical-conical bone defect, measuring 3 mm in diameter and 5 mm in depth, at the distal end of the femur. The surgical site was then meticulously sutured in layers to ensure proper wound closure, and the animals were monitored for any signs of infection or ecchymosis. The absence of such complications indicated the successful establishment of a rat model featuring a bone defect at the distal femur.

The rats with successfully established models were randomly assigned to 4 distinct groups, each comprising 8 rats. The first group served as the control, receiving 100 μL PBS intervention. The second group was the CSMA hydrogel group, in which 100 μL CSMA hydrogel was administered via syringe injection. The third group was the CSMA + Norm-exo group, where 100 μL CSMA hydrogel encapsulating Norm-exo with 20 μg protein was injected using a syringe. The fourth group was the CSMA + Elec-exo group, involving the injection of 100 μL CSMA hydrogel containing Elec-exo with 20 μg protein, also delivered by syringe.

2.14. In vivo hard tissue regeneration at bone defect sites

At 4- and 8-weeks following implantation, three rats from each group were euthanized. The femurs were harvested and fixed in a 10 % neutral buffered formalin solution for 48 h. Subsequently, all specimens underwent scanning and analysis using the Bruker Skyscan 1276 Micro-CT. We used Dataviewer to split the Micro-CT images into three orthogonal views and saved the x-z and y-z axis slice images, which were then colorized using the default color palette provided by the software. The three-dimensional images were reconstructed with CTvox software, focusing on the defect site as the center. The relative bone volume fraction (BV/TV) and bone mineral density (BMD) for each group were calculated using CTan software. The region of interest (ROI) was delineated as the half-side bone tissue surrounding the bone defect site in the y-z axis slices.

2.15. In vivo histological staining at bone defect sites

Following a 6-week implantation period, two rats were euthanized. Their tissues were subsequently fixed and embedded, and hard tissue sections were prepared. These sections underwent hematoxylin and eosin (HE) staining, Masson's trichrome staining, and immunohistochemical staining for osteocalcin (OCN). The sections were dewaxed and rehydrated, then treated with 0.4 % pepsin at 37 °C for 20 min to facilitate enzymatic repair. Following this, the sections were blocked with 3 % hydrogen peroxide and 1 % bovine serum albumin (BSA) solution. They were then co-incubated with the primary antibody, specifically the OCN primary antibody from Beyotime, China. DAB was utilized as the chromogen, and the sections were counterstained with hematoxylin. Finally, the sections were mounted and examined under an optical microscope to capture detailed images [42].

3. Results and discussion

3.1. Preparation of electrical stimulated rat bone mesenchymal stem cells

We first isolated RBMSCs according to the method described in reference [41], and selected the third generation of cells with strong growth and uniform morphology. In order to harvest mesenchymal stem cells with different current intensities, we randomly divided the cells into 4 groups and placed them in the same self-made electrical stimulation Petri dish. According to previous literature reports [43,44], the suitable electrical stimulation intensity was 10–200 μA. Therefore, as illustrated in the schematic diagram in Fig. 1A, we controlled the current intensity for each group to 0, 20, 75, and 150 μA, respectively, by adjusting the resistance in the total circuit. To achieve a more pronounced stimulation effect, we set the stimulation program at 1 h per day for a continuous period of 5 days. Fortunately, there was no significant change in the temperature of the culture dish before and after the 1-h electrical stimulation (Figs. S1 and S2). Subsequently, after the optimal stimulation intensity was determined in subsequent experiments, we conducted transcriptome sequencing analysis on BMSCs following various treatments. We set the criteria for differential gene expression as a fold change (FC) of ≥ 2 or ≤ 0.5 (i.e., $|\log2(FC)| \geq 1$) and a p-value of <0.05. Among the 15,165 genes analyzed, 817 were differentially expressed. Compared to Norm-BMSCs, the group of Elec-BMSCs upregulated 329 genes and downregulated 488 genes, as shown in Fig. 1B. We generated a heatmap of the top 50 differentially expressed genes (Fig. 1C). According to the results of differentially expressed genes, Col2a1, which is related to ECM-receptor interaction, was highly increased in Electrical stimulated-BMSCs, confirming that electrical stimulation can increase the ability of BMSCs to regenerate bone.

3.2. Preparation and characterization of Norm-exo and Elec-exo

Typically, exosome isolation methods encompass

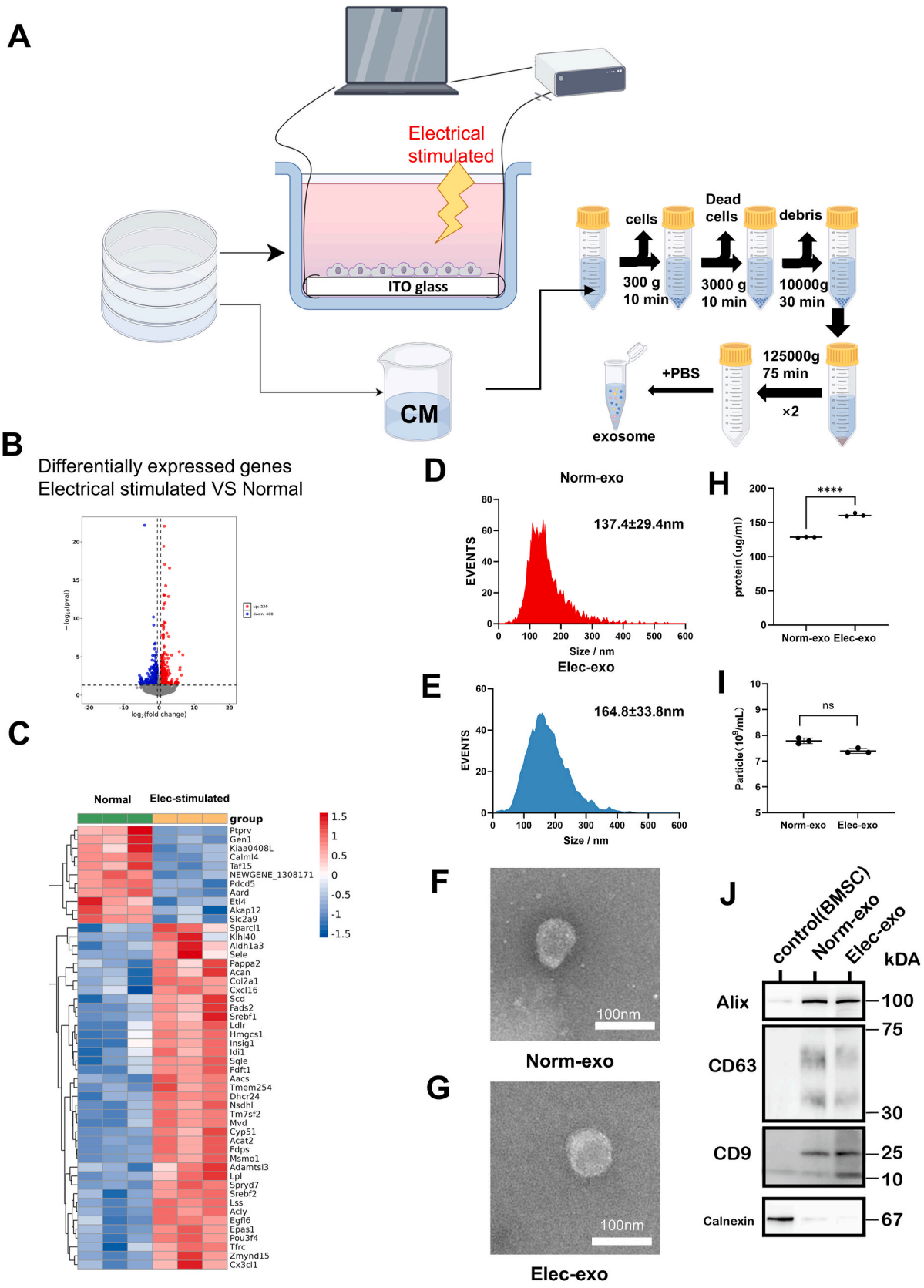

Fig. 1. Characterization analysis of electrically stimulated BMSCs and their derived exosomes compared to the normal group. A) Schematic diagram of the device for electrically stimulating mesenchymal stem cells and the process of exosome isolation and purification. (By Figdraw) B) Venn diagram illustrating the differentially expressed genes in Elec-BMSCs relative to Norm-BMSCs. C) Heatmap depicting the clustering of differentially expressed genes. D). E) The particle size and distribution of Norm - exo and Elec – exo by nanoparticle tracking analysis (NTA). F). G) Transmission electron microscopy (TEM) images of Norm - exo and Elec - exo. H) Exosome protein concentration and I) particle number in the two groups per unit solution, n = 3. J) Western Blot results for exosome surface protein markers (Alix, CD63, CD9 and Calnexin). Results are shown as mean ± standard deviation (SD). Significance is indicated by ****$p < 0.001$.

ultracentrifugation, polymer precipitation, ultrafiltration, and microfluidics. As depicted in Fig. 1 A, gradient ultracentrifugation was utilized in this study to isolate and purify exosomes from Elec-BMSCs and Norm-BMSCs. The average particle size of Norm-exo was found to be slightly smaller than that of Elec-exo, as determined by nanoparticle tracking analysis (NTA). (137.4 ± 29.4 nm for Norm-exo versus 164.8 ± 33.8 nm for Elec-exo) (Fig. 1DE). Moreover, the Z-average results from DLS (157.63 ± 2.43 nm for Norm-exo and 163.2 ± 1.8 nm for Elec-exo) also demonstrated that electrical stimulation pre-treatment does not affect the average size of exosomes (Figure S2AB).Transmission electron microscopy (TEM) images revealed the characteristic cup-shaped morphology of the exosomes (Fig. 1FG). The larger exosome particle size affords additional space for the encapsulation of proteins and other cargoes. Fig. 1H and I illustrate that Elec-exo contains a higher protein concentration per unit volume of exosome solution. Western blot analysis showed a marked increase in surface markers, including CD9, CD63, Alix and Calnexin proteins, on the isolated nanoparticles compared to BMSCs (Fig. 1J). Collectively, these findings confirm the successful isolation of exosomes derived from both untreated electrically stimulated BMSCs using gradient ultracentrifugation.

3.3. The effects of different types and concentrations of Elec-exo on the proliferation, osteogenic induction and mineralization of ROBs and RBMSCs

In order to screen for the optimal current intensity of electrical stimulation, we added the exosomes extracted from each group to the culture dishes containing RBMSCs and ROBs, respectively (Fig. 2 A). The results of the CCK-8 cell proliferation assay showed that Elec-exo at 75 μA and 150 μA significantly enhanced the proliferation of ROBs. In contrast, there was no significant difference in the effect of any exosome treatment on the proliferation of BMSCs. (Fig. 2 BC). We detect the expression levels of osteogenesis-related genes Bmp2, Col1A1, and Opn by RT-qPCR. As shown in Fig. 2 DE, after 48 h of exosome treatment, the expression of these three genes was significantly upregulated in ROBs and RBMSCs co-incubated with exosomes pre-treated with 150 μA electrical stimulation. This result indicates that 150 μA electrical stimulation group are most effective in promoting cell osteogenic differentiation. After 7 days of co-incubation, it is possible to deduce that 150 μA group electrical stimulation could significantly enhance the ALP activity of ROBs from staining results (Fig. 2F and G). After 21 days of co-incubation, we can infer from ARS staining that the area of calcium nodules deposited in the 75 μA group was larger than that in the control group (Fig. 2H and I). Based on the literature reports and the above experimental results, we believe that 150 μA is the appropriate intensity for electrical stimulation pre-treatment.

In subsequent experiments, we used exosomes derived from BMSCs pre-treated with 150 μA electrical stimulation as Elec-exo, and exosomes derived from BMSCs without electrical stimulation pre-treatment as Norm-exo. According to the literature, the optimal concentration of exosome protein for in vitro co-culture with ROBs is 5–20 μg/mL. To explore the effect of exosome concentration on the osteogenic mineralization capabilities of ROBs, we continued to co-incubate ROBs with different concentrations of Elec-exo and Norm-exo. RT-qPCR results showed that concentrations of Elec-exo at 20 μg/mL and above could promote the expression of osteogenesis-related genes (Fig. 3B–D). The results of ALP and ARS staining also indicated that a concentration of 10–20 μg/mL was more effective in promoting bone regeneration. In particular, at the same concentration, 10 μg/mL Elec-exo induced ALP expression and ARS were significantly higher than Norm-exo, further confirming that Elec-exo induces osteogenic induction and mineralization capabilities of ROBs better than Norm-exo.

3.4. Synthesis and Characterization of CSMA

The schematic diagram of CSMA synthesis is presented in Fig. 4A, whereas Fig. 4B displays the SEM images of the lyophilized CSMA hydrogel and the lyophilized CSMA hydrogel loaded with exosomes. In addition, we captured images of the CSMA hydrogel loaded with PKH26-stained exosomes under both bright-field and fluorescence microscopy (Fig. S3). These results collectively demonstrate the successful loading of exosomes. The cell viability of BMSCs co-incubated with different concentrations of CSMA was evaluated by CCK-8 method. As depicted in Fig. 4C, the incorporation of CSMA significantly enhanced the viability of BMSCs after a 2-day co-incubation period. Notably, the group co-incubated with a 7 % concentration of CSMA showed the most pronounced difference. Live/dead staining further corroborated that CSMA markedly stimulated the proliferation of ROBs and BMSCs, as illustrated in Fig. 4D. These results indicate that CSMA has good cytocompatibility and can promote the proliferation of BMSCs.

we can use a 405 nm laser emitter to irradiate the syringe for 30 s and directly inject the mixture into the target site (Fig. 4E). The in vitro release profile of exosomes in CSMA hydrogels was evaluated. As shown in Fig. 4 F, t the release of exosomes lasted for about 2 weeks. On the 14th day, the cumulative release of exosomes was 88.4 %. The results of in vivo fluorescence imaging also confirmed that the release of exosomes lasted for about 2 weeks, with the majority of exosomes being metabolized by the liver after entering the circulation (Fig. 4G).

3.5. Proteomic differences and bioinformatics analysis of Norm-exo and Elec-exo

Exosomes are rich in a diverse array of proteins, which hold the potential to influence a myriad of biological processes [45]. Delving deeper into the compositional disparities between Norm-exo and Elec-exo, we embarked on a proteomic analysis of these two exosome types.

Our findings revealed a significant proteomic shift in the Elec-exo group when juxtaposed against the Norm-exo cohort, with a total of 1467 proteins exhibiting altered expression levels—comprising 1447 proteins that were upregulated and 20 that were downregulated (Fig. 5A). This aligns with the elevated protein content observed in the Elec-exo group through BCA quantification (Fig. 1H), suggesting a richer protein content within Elec-exo, indicative of heightened biological activity. We calculated the Pearson correlation coefficients (PCC) between all samples based on their intensity values and generated a visualized heatmap (Fig. S4b). Additionally, to ensure the quality of the sequencing results, we also performed principal component analysis (PCA) (Fig. S4a).

From the heatmap of the top 50 differentially expressed genes in Fig. 5C, we identified an interesting protein: Stc2. STC2 may promote the proliferation and differentiation of osteoblasts during bone regeneration by regulating extracellular calcium ion levels and the release of growth factors [46]. Additionally, it may indirectly affect oxidative phosphorylation by modulating mitochondrial function [47]. To further explore the functional significance of these differences, we performed Gene Ontology (GO) enrichment analysis on the set of differentially expressed proteins (DEPs). The GO analysis classified proteins according to biological processes, molecular functions, and cellular components (Fig. 5D–F). The findings revealed the proteins' involvement in processes such as " Oxidative phosphorylation " and "calcium ion binding." The upregulation of translation-related proteins facilitates the proliferation and differentiation of effector cells. The increase in calcium ion binding-related proteins serves as a precursor to cell mineralization. Moreover, we conducted Kyoto Encyclopedia of Genes and Genomes (KEGG) pathway enrichment analysis on the DEPs (Fig. 5G). Additionally, we performed GSEA analysis targeting the Oxidative phosphorylation pathway using protein sets defined by GO or KEGG terms, focusing on proteins with expression changes, and the results showed significant differences. The results indicated that these proteins are involved in regulating the "Oxidative phosphorylation" pathway (Fig. S4c.S4d).

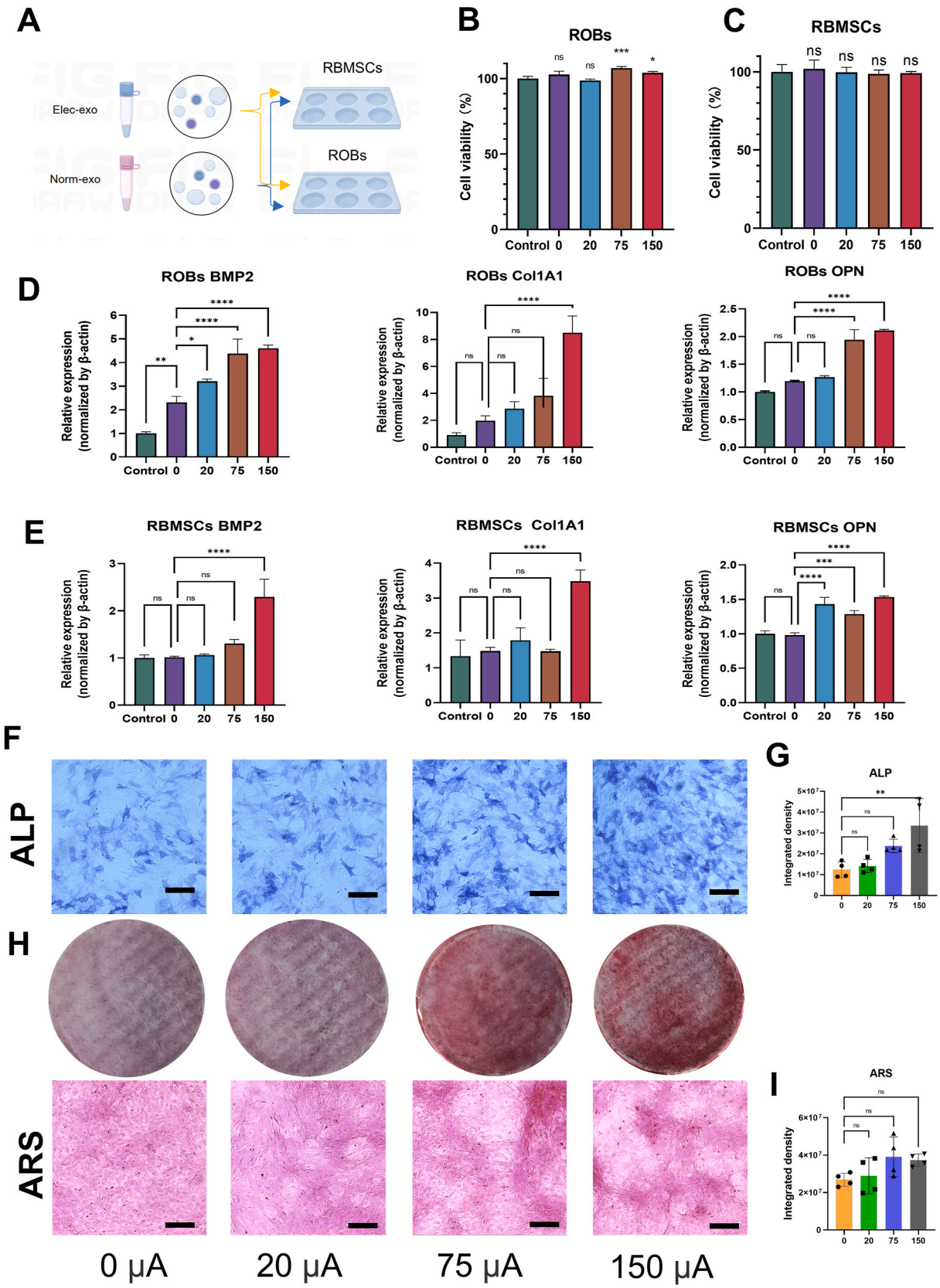

Fig. 2. Proliferation, osteogenic induction and mineralization of ROBs and RBMSCs induced by different types of Elec-exo. A) Schematic representation of the treatment of ROBs and RBMSCs with Norm-exo and Elec-exo (By Figdraw). B). C) Cell proliferation detected by CCK-8 assay, n = 5. D). E) Expression levels of genes associated with osteogenesis. (Bmp2, Col1A1, and Opn) in ROBs and RBMSCs detected by RT-qPCR on day 2, n = 3. F) ALP staining of ROBs (scale bar represents 100 μm) G) Corresponding quantitative analysis of integrated density values, n = 4. H) ARS staining after co-incubation for 21 days (scale bar represents 100 μm) I) Analysis of integrated density values, n = 4. Results are shown as mean ± SD. ns: non-significant differences, *p < 0.05, **p < 0.01, ***p < 0.001, ****p < 0.0001.

A

Protein (μg/mL)	Particles/mL (Norm-exo)	Particles/mL (Elec-exo)
0	0	0
5	$2.87*10^9$	$2.44*10^9$
10	$5.74*10^9$	$4.88*10^9$
20	$1.15*10^{10}$	$9.76*10^9$

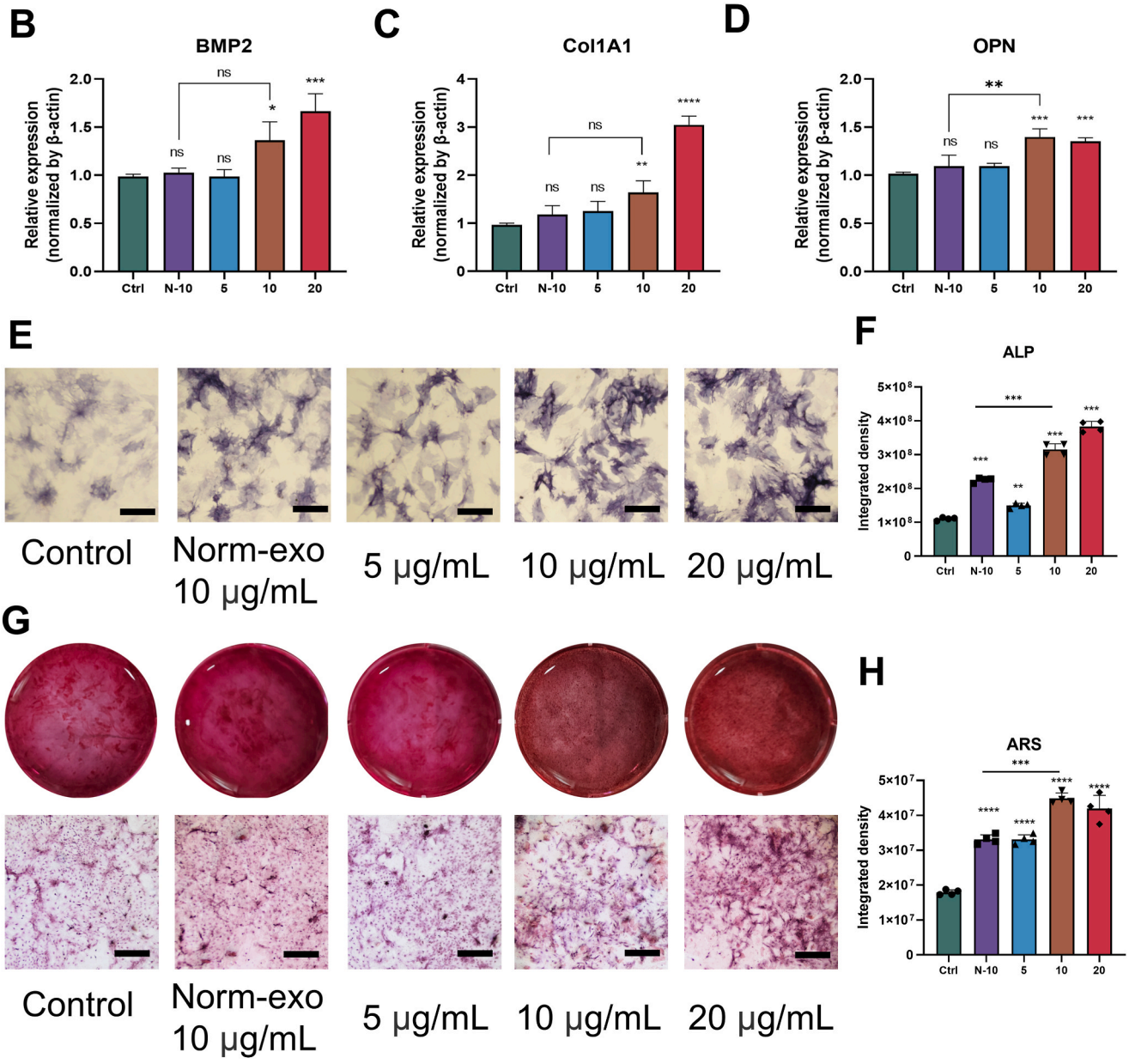

Fig. 3. Differentiation and mineralization of ROBs induced by different doses of Elec-exos. A) Table of correspondence between the number of exosomes particles and protein content B). C). D). Expression of Bmp2, Col1A1 and Opn genes of ROBs by RT-qPCR, n = 3. N-10 showed Norm-exo with 10 μg/mL E) ALP staining of ROBs (scale bar represent 20 μm) F) Corresponding quantitative analysis of integrated density values, n = 4. G) ARS staining of ROBs (scale bar represent 200 μm) H) Analysis of integrated density values, n = 4. Results are shown as mean ± SD. ns: non-significant differences, *p < 0.05, **p < 0.01, ***p < 0.001, ****p < 0.0001.

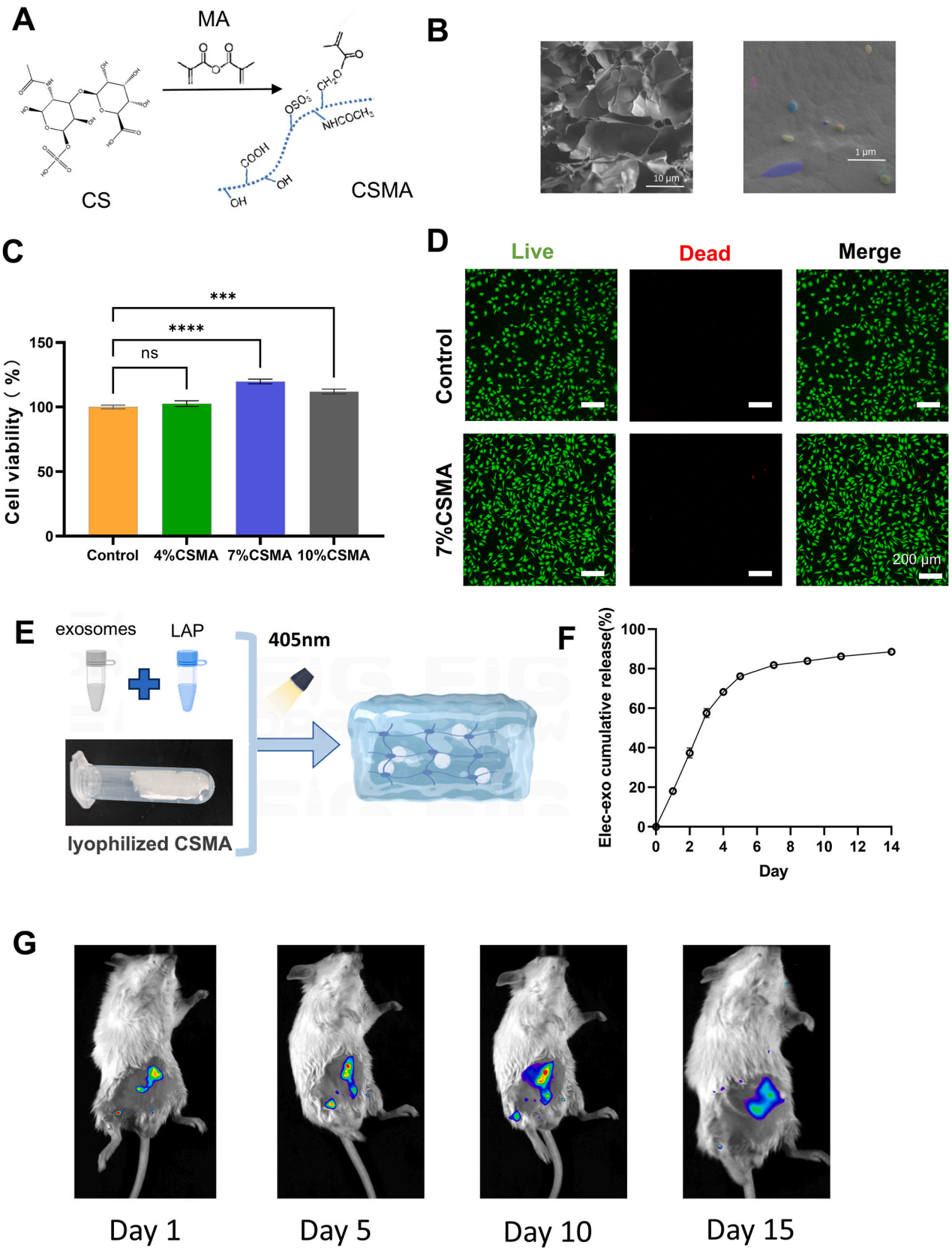

Fig. 4. Synthesis and Characterization of CSMA. A) Schematic diagram of CSMA synthesis B) SEM of lyophilized CSMA hydrogel and lyophilized CSMA hydrogel loaded with exosomes. C) Cell proliferation detected by CCK-8 assay, n = 5. D) Live/Dead staining of RBMSCs after a 2-day co-incubation period with 100 μg 7 % CSMA hydrogel. E) Schematic diagram of mixing and photocuring of exosome and CSMA hydrogel precursor solution (By Figdraw.) F) In vitro exosomes release profiles n = 3. G) Fluorescence distribution in mice. Results are shown as mean ± SD. ns: non-significant differences, ***p < 0.001, ****p < 0.0001.

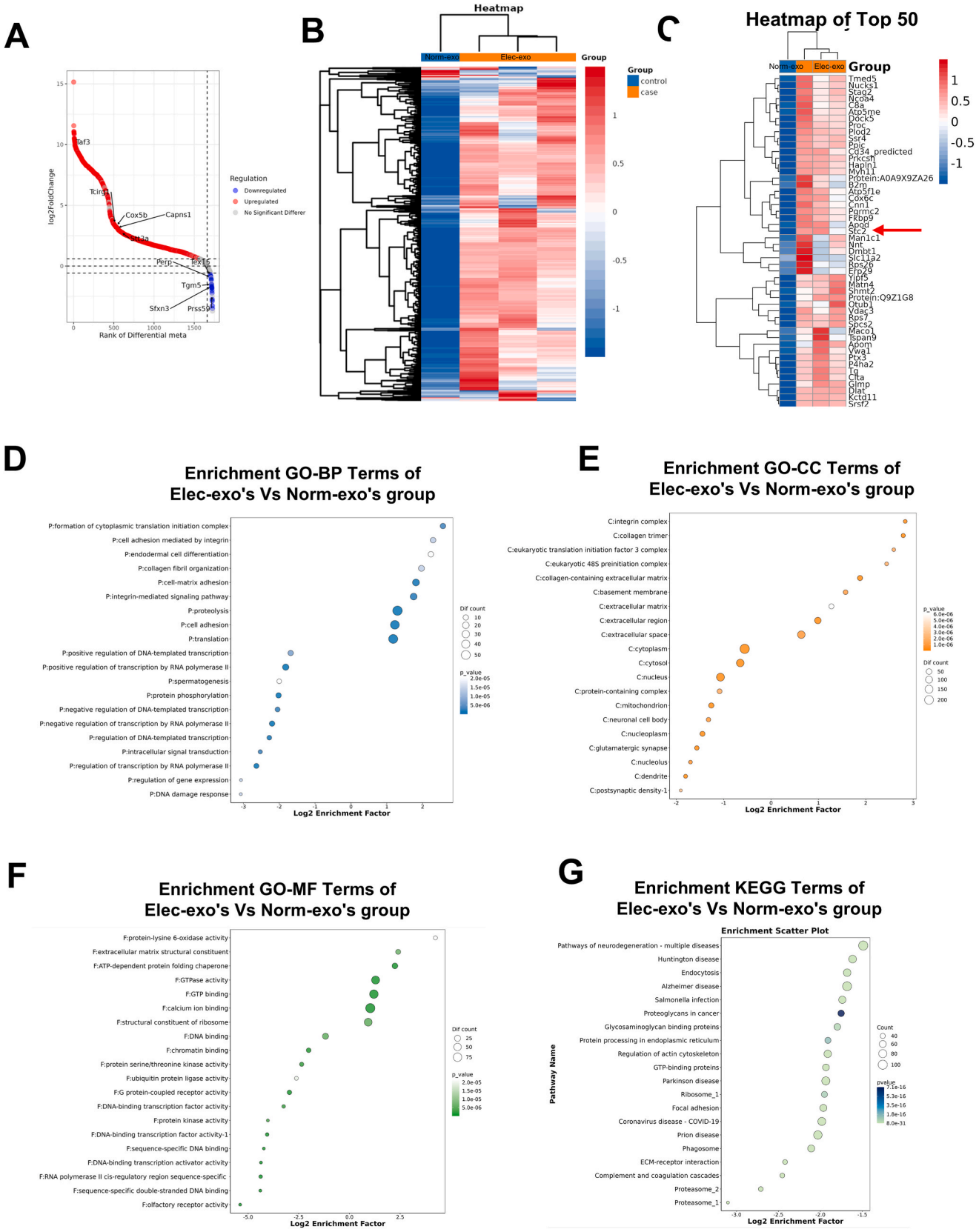

Fig. 5. Proteomic sequencing results of Norm-exo and Elec-exo. A) Volcano plot of proteins in Elec-exo and Norm-exo B.C) Heatmap of total and top 50 different proteins of two groups. (D–F) GO enrichment analysis (Biological Process (GO-BP), Cellular Component (GO-CC), and Molecular Function (GO-MF)) and (G) Enrichment KEGG analysis of the differentially expressed proteins.

Collectively, these results suggest that preconditioning with electrical stimulation modulates the levels of functional proteins in stem cell-derived exosomes, thereby enriching the content of functional proteins in Elec-exo. The increase in functional protein content is likely to play a pivotal role in various biological activities such as signal transduction and calcium ion metabolism in bone tissue, thereby enhancing the therapeutic potential of Elec-exo in bone tissue regeneration.

3.6. Differential transcriptomic expression differences and bioinformatics analysis in BMSCs treated with Norm-exo and Elec-exo

To further investigate the regulatory effects of Norm-exo and Elec-exo, we conducted transcriptomic analysis on the three groups of cells. Similar to proteomics analysis, first, we generated a PCA plot (Fig. S5a) and a heatmap visualizing the PCC values (Fig. S5b). When comparing differentially expressed genes (DEGs), as shown in Fig. 6A, the Norm-exo group exhibited differential expression in 1400 genes compared to the Control group, comprising 389 upregulated and 1011 downregulated genes (Fig. 6B). Meanwhile, the Elec-exo group displayed differential expression in 1038 genes, with 304 upregulated and 734 downregulated genes (Fig. 6C). Additionally, when comparing the Elec-exo group to the Norm-exo group, we found that the Elec-exo group had 203 genes with changed expression levels, consisting of 115 upregulated genes and 88 downregulated genes (Fig. 6C).

We have also illustrated the differentially expressed genes (DEGs) across the three groups in Fig. 6E, and listed the Top 50 DEGs from pairwise comparisons in Fig. S5c–e.

Based on GO enrichment analysis, we found that both Elec-exo and Norm-exo are involved in modulating a series of processes related to bone tissue regeneration, such as "ossification " and so on, especially in Elec-exo group (Fig. 6F–H). We also conducted KEGG analysis on these groups. Contrasted with the control, Elec-exo were associated with the "PI3K-Akt signaling pathway" and "MAPK signaling pathway," both of which are vital for various cellular functions, including growth, survival, and osteogenic differentiation. In comparison, Elec-exo, compared to the Norm-exo group, regulated the " Pl3k-Akt signaling pathway", "ECM-receptor interaction" and "Cytoskeleton in muscle cells", which are associated with the osteogenic differentiation of stem cells (Fig. 6F–H). Therefore, we performed Western Blot (WB) detection of the signature proteins Akt and p-Akt in the PI3K-Akt signaling pathway. The experimental results showed that Elec-exo can indeed promote bone regeneration by activating the PI3K-Akt signaling pathway (Fig. 6D). To verify the universality of Elec-exo in activating the PI3K-Akt signaling pathway, we also performed Western Blot detection on ROBs under different interventions (Fig. S6). The results similarly confirmed the activation of the PI3K-Akt signaling pathway. To further highlight the differences in the modulatory effects of Norm-exo and Elec-exo, we also performed a gene set enrichment analysis (GSEA). However, no pathway showed a significant difference.

3.7. In vivo bone tissue regeneration at defect sites

The cylindrical-conical defect with a diameter of 3 mm and a depth of 5 mm was constructed with a Kirschner wire on the distal femur of SD rats and the PBS or CSMA hydrogel or CSMA hydrogel loaded with different exosomes was injected the next day. Fig. 7A outlines the treatment protocol. After 4 and 8 weeks of treatment, the animals were humanely sacrificed, and their femurs were harvested for micro-CT analysis. At 6 weeks post-intervention, the femurs were extracted for histological and immunohistochemical analyses. These analyses were conducted to evaluate the bone repair efficacy and in vivo biocompatibility of the CSMA hydrogel loaded with different exosomes. From the Micro-CT images and reconstructed images of the vertical and horizontal cross sections of the defect site, it can be seen that the CSMA + Elec-exo group showed the strongest bone repair ability in all groups (Fig. 7BC). Further quantitative analysis of Micro-CT image images obtained four indicators reflecting the quality of new bone regeneration: the percentage of bone volume to total volume (BV/TV) and bone mineral density (BMD). As shown in Fig. 7D, at the eighth week, the BV/TV value of the CSMA + Elec-exo group reached 83.30 ± 2.78 %, which was significantly higher than that of the control group and the Blk-CSMA group (control group 43,74 ± 2.67 %, Blk-CSMA group 64.08 ± 5.19 %, CSMA + Norm-exo group 83.02 ± 2.49 %). At the same time, the BV/TV value of the CSMA + Elec-exo group reached 79.04 ± 6.40 % at 4 weeks, which was significantly higher than that of the other three groups (Control group 38.18 ± 5.73 %, Blk-CSMA group 45.20 ± 5.85 %, CSMA + Norm-exo group 61.34 ± 5.99 %). This shows that CSMA + Elec-exo not only has the strongest bone repair ability, but also can accelerate bone regeneration and repair bone defects faster in a shorter time.

Regarding the in vivo experimental results at week 8, compared with the hydrogel loaded with Norm-exo, the hydrogel loaded with Elec-exo did not show a significant acceleration effect. There may be several reasons for this.

1. At week 4, the BV/TV value of the CSMA + Elec-exo group had already reached as high as 79.04 ± 6.40 %, which was significantly different from the other groups. It may have entered the bone remodeling phase earlier in the following four weeks, resulting in little change in BMD and BV/TV values at week 8, thus giving other groups the opportunity to catch up.
2. From the results of Fig. 4F and G, it can be seen that the exosomes in the hydrogel had already been metabolized by weeks 2–3. Therefore, the healing of bone tissue in the following four weeks may have been less influenced by the material, which could also be a possible reason for this conclusion.
3. We chose the simple and convenient distal femoral bone defect model instead of the cranial large segmental bone defect model. In terms of the inherent regenerative capacity of bone tissue, the regeneration ability of distal femoral fractures is definitely much greater than that of cranial bone defects. Similar studies in the literature used two time points of 2W and 4W. In future experiments, we will take into account various factors to better demonstrate the excellent osteogenic ability of the CSMA + Elec-exo group.

We also performed histological analysis by Masson trichrome staining, H & E staining and OCN immunohistochemical staining (Fig. 8). As shown in Fig. 8B–D, the mature bone area of the CSMA + Elec-exo group was much larger than that of the other three groups, indicating that the CSMA + Elec-exo group had the strongest bone repair ability. Furthermore, as depicted in Fig. 8C–E, the bone defect site in the CSMA + Elec-exo group exhibited a highly conspicuous region of elevated expression of the osteogenesis-related protein OCN, suggesting that this group demonstrated the highest level of osteogenic activity. These positive results together indicate that the continuous delivery of Elec-exo mediated by active CSMA hydrogel scaffold exhibits the best osteogenic ability in vivo.

4. Conclusion

In this study, an injectable CSMA hydrogel loaded with Elec-exo was developed for bone regeneration. The BMSC-derived exosomes pretreated by electrical stimulation significantly promoted the proliferation of osteoblasts and the osteogenic differentiation of bone marrow mesenchymal stem cells, and showed good bone regeneration effect in vitro and in vivo. Proteome and transcriptome analysis showed that Elec-exo mainly promoted bone regeneration by activating Pl3k-Akt and MAPK bone formation-related signaling pathways. Therefore, we firmly believe that our study can broaden the therapeutic application of exosomes in accelerating bone regeneration.

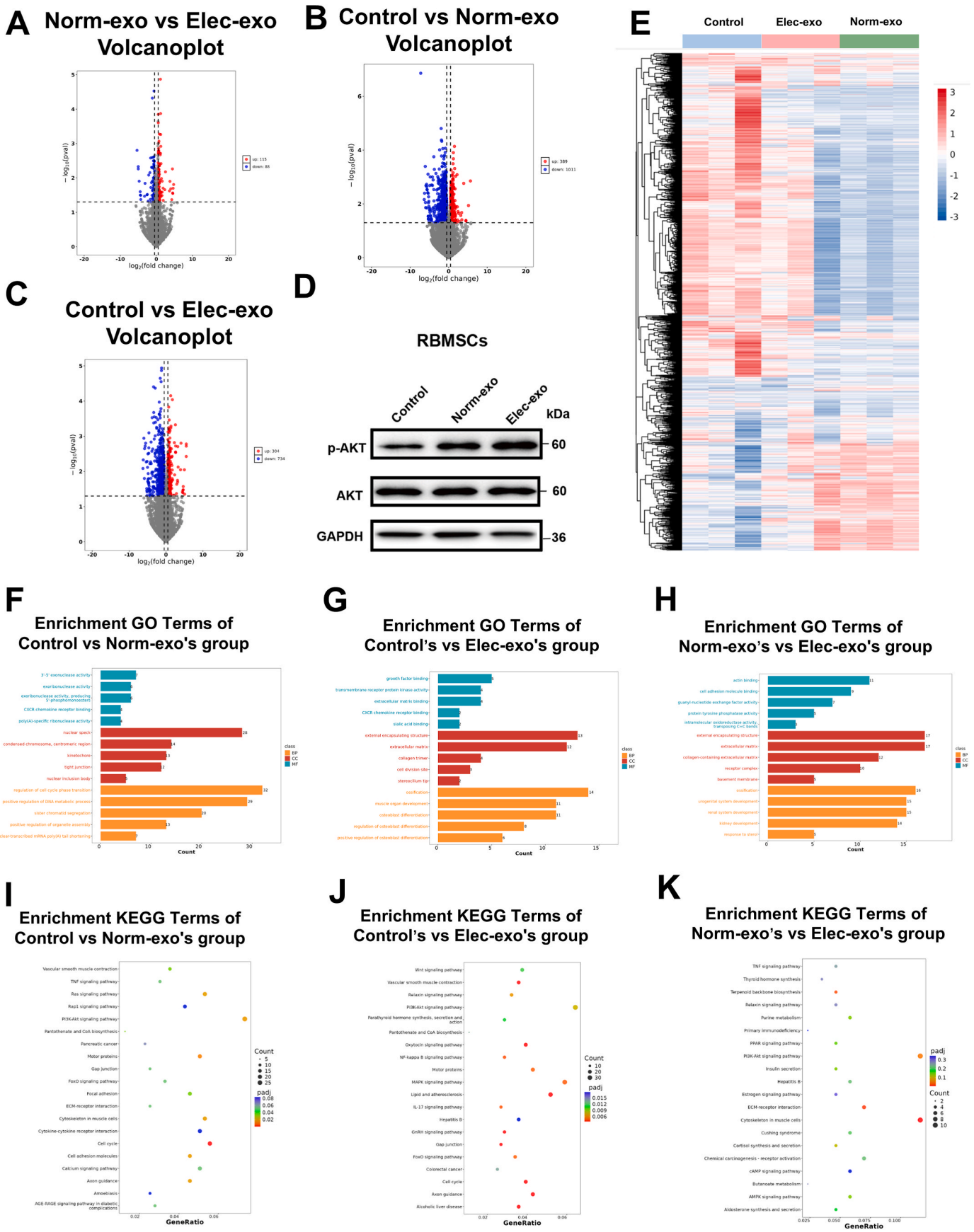

Fig. 6. mRNA sequencing and differential gene expression analysis of the three BMSC groups. (A–C) Volcano plots and heatmaps (E) illustrating the differentially expressed genes (DEGs) across the three groups. D) Verification of the activation of the PI3K-Akt signaling pathway in RBMSCs by WB. F-K)Enrichment GO and KEGG analysis of the Norm-exo's group vs Control group (F, I), Elec-exo's group vs Control group (G, J), and the Elec-exo's group vs Norm-exo's group (H, K).

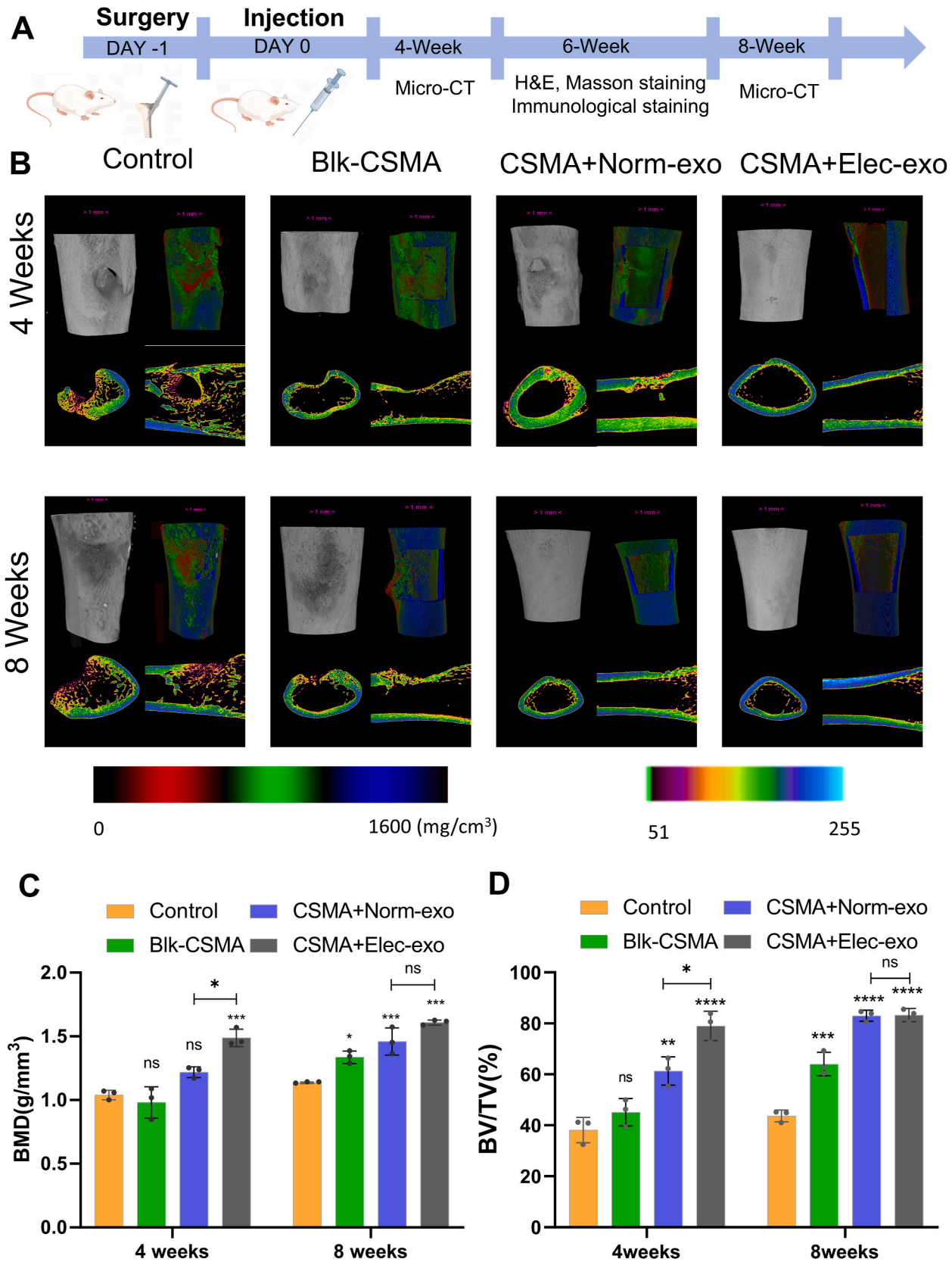

Fig. 7. In vivo regeneration of the distal femur. A) Schematic representation of the treatment timeline (By Figdraw). B) Micro CT and 3D reconstruction images of the distal femur defect site at 4- and 8-weeks post-injection. C,D) Quantitative measurements of bone volume fraction (BV/TV) and bone mineral density (BMD), with n = 3. Results are shown as mean ± SD. *p < 0.05, **p < 0.01, ***p < 0.001, ****p < 0.0001.

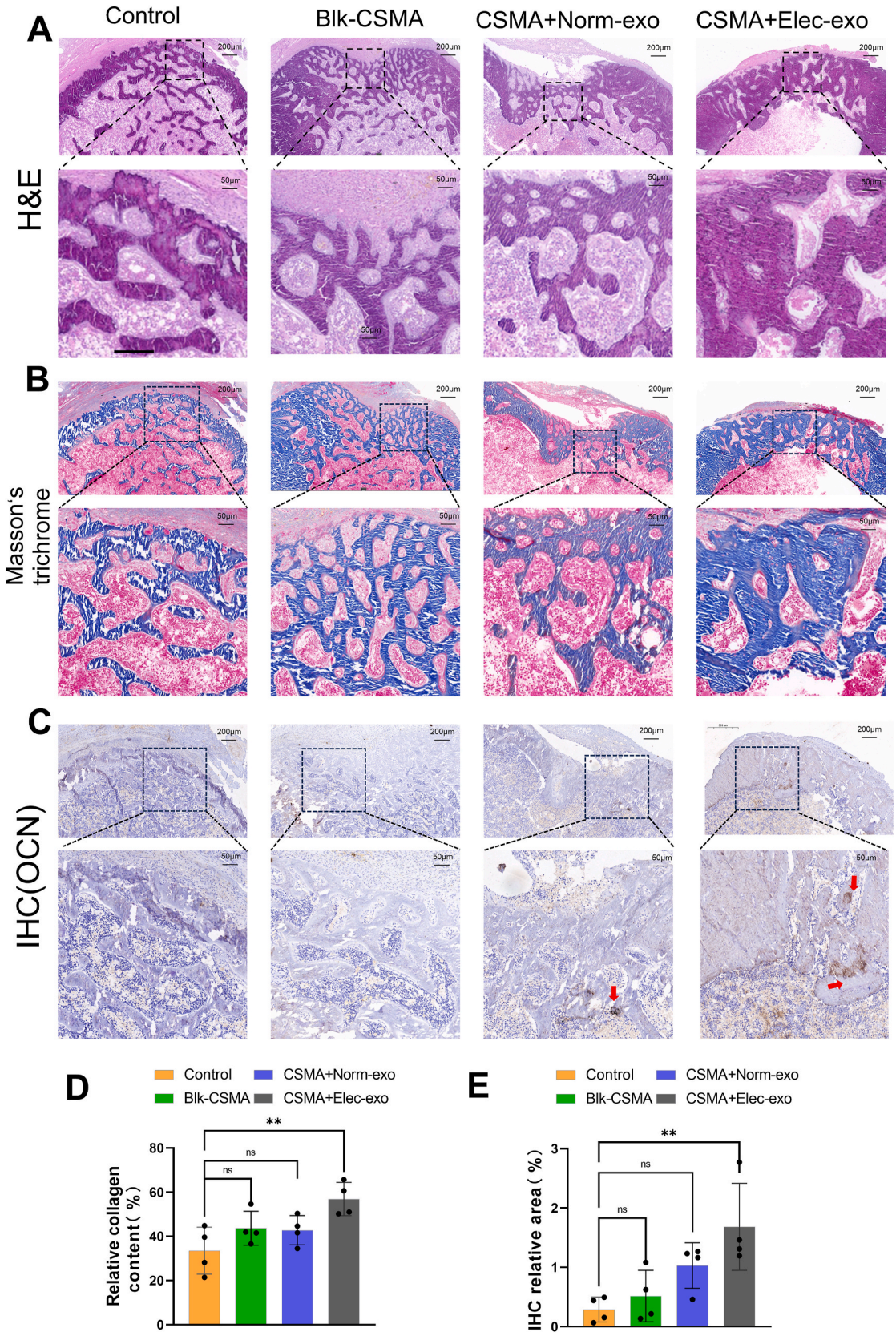

Fig. 8. Histological staining of the distal femur defect site at 6-weeks post-injection. (A) Hematoxylin and eosin (H&E) staining, (B) Masson's trichrome staining, and (C) Immunohistochemical staining for OCN. D) The relative proportion of collagen from the quantitative analysis of Masson staining. E) Quantitative analysis results of IHC Results are shown as mean ± SD. ns: non-significant differences, **$p < 0.01$.

CRediT authorship contribution statement

Jialu Chen: Writing – original draft, Investigation, Data curation, Conceptualization. **Jian Chen:** Methodology, Investigation, Formal analysis. **Jiahao Chen:** Validation, Software, Data curation. **Renjie Lu:** Visualization, Software. **Ziyuan Liu:** Methodology. **Yang Zhang:** Supervision. **Chi Zhang:** Writing – review & editing, Supervision.

Ethics approval and consent to participate

All the animal procedures were performed under the protocols approved by the Animal Welfare Ethics Committee of Shanghai Tenth People's Hospital (SHDSYY-2023-4443-2).

Declaration of competing interest

The authors declare that they have no known competing financial interests or personal relationships that could have appeared to influence the work reported in this paper.

Acknowledgements

Jialu Chen, Jiahao Chen and Jian Chen contributed equally to this work. This work was supported by Shanghai Magnolia Talent Plan Pujiang Project, Shanghai, China (21PJD052).

Appendix A. Supplementary data

Supplementary data to this article can be found online at https://doi.org/10.1016/j.bioactmat.2025.04.019.

References

[1] Q. Zhu, Y. Tang, T. Zhou, L. Yang, G. Zhang, Y. Meng, H. Zhang, J. Gao, C. Wang, Y. X. Su, J. Ye, Exosomes derived from mesenchymal stromal cells promote bone regeneration by delivering miR-182-5p-inhibitor, Pharmacol. Res. 192 (2023) 106798, https://doi.org/10.1016/j.phrs.2023.106798.

[2] A. Saberi, M. Kouhjani, M. Mohammadi, L. Hosta-Rigau, Novel scaffold platforms for simultaneous induction osteogenesis and angiogenesis in bone tissue engineering: a cutting-edge approach, J. Nanobiotechnol. 21 (2023) 351, https://doi.org/10.1186/s12951-023-02115-7.

[3] X. Song, L. Xu, W. Zhang, Biomimetic synthesis and optimization of extracellular vesicles for bone regeneration, J. Control. Release 355 (2023) 18–41, https://doi.org/10.1016/j.jconrel.2023.01.057.

[4] B.C. Heng, Y. Bai, X. Li, L.W. Lim, W. Li, Z. Ge, X. Zhang, X. Deng, Electroactive biomaterials for facilitating bone defect repair under pathological conditions, Adv. Sci. 10 (2023) e2204502, https://doi.org/10.1002/advs.202204502.

[5] Y. Tang, C. Wu, Z. Wu, L. Hu, W. Zhang, K. Zhao, Fabrication and in vitro biological properties of piezoelectric bioceramics for bone regeneration, Sci. Rep. 7 (2017) 43360, https://doi.org/10.1038/srep43360.

[6] X. Kong, T. Zheng, Z. Wang, T. Zhou, J. Shi, Y. Wang, B. Zhang, Remote actuation and on-demand activation of biomaterials pre-incorporated with physical cues for bone repair, Theranostics 14 (2024) 4438–4461, https://doi.org/10.7150/thno.97610.

[7] S. Zhang, L. Huang, M. Bian, L. Xiao, D. Zhou, Z. Tao, Z. Zhao, J. Zhang, L.B. Jiang, Y. Li, Multifunctional bone regeneration membrane with flexibility. Electrical Stimulation Activity and Osteoinductive Activity, Small, 2024 e2405311, https://doi.org/10.1002/smll.202405311.

[8] C. Yu, X. Ying, M.A. Shahbazi, L. Yang, Z. Ma, L. Ye, W. Yang, R. Sun, T. Gu, R. Tang, S. Fan, S. Yao, A nano-conductive osteogenic hydrogel to locally promote calcium influx for electro-inspired bone defect regeneration, Biomaterials 301 (2023) 122266, https://doi.org/10.1016/j.biomaterials.2023.122266.

[9] E. Fukada, I. Yasuda, On the piezoelectric effect of bone, J. Phys. Soc. Jpn. 12 (1957) 1158–1162, https://doi.org/10.1143/Jpsj.12.1158.

[10] J. Tang, A. Vandergriff, Z. Wang, M.T. Hensley, J. Cores, T.A. Allen, P.U. Dinh, J. Zhang, T.G. Caranasos, K. Cheng, A regenerative cardiac patch formed by spray painting of biomaterials onto the heart, Tissue Eng. C Methods 23 (2017) 146–155, https://doi.org/10.1089/ten.TEC.2016.0492.

[11] Y. Xie, A. Ibrahim, K. Cheng, Z. Wu, W. Liang, K. Malliaras, B. Sun, W. Liu, D. Shen, H. Cheol Cho, T. Li, L. Lu, G. Lu, E. Marban, Importance of cell-cell contact in the therapeutic benefits of cardiosphere-derived cells, Stem Cell. 32 (2014) 2397–2406, https://doi.org/10.1002/stem.1736.

[12] Z. Li, S. Hu, K. Huang, T. Su, J. Cores, K. Cheng, Targeted anti-IL-1beta platelet microparticles for cardiac detoxing and repair, Sci. Adv. 6 (2020) eaay0589, https://doi.org/10.1126/sciadv.aay0589.

[13] F. Liu, S. Hu, S. Wang, K. Cheng, Cell and biomaterial-based approaches to uterus regeneration, Regen. Biomater. 6 (2019) 141–148, https://doi.org/10.1093/rb/rbz021.

[14] H. Liu, X. Zhang, M. Zhang, S. Zhang, J. Li, Y. Zhang, Q. Wang, J.P. Cai, K. Cheng, S. Wang, Mesenchymal stem cell derived exosomes repair uterine injury by targeting transforming growth factor-β signaling, ACS Nano 18 (2024) 3509–3519, https://doi.org/10.1021/acsnano.3c10884.

[15] K.D. Popowski, B. López de Juan Abad, A. George, D. Silkstone, E. Belcher, J. Chung, A. Ghodsi, H. Lutz, J. Davenport, M. Flanagan, J. Piedrahita, P.-U. C. Dinh, K. Cheng, Inhalable exosomes outperform liposomes as mRNA and protein drug carriers to the lung, Extracellular Vesicle 1 (2022) 100002, https://doi.org/10.1016/j.vesic.2022.100002.

[16] X. Wang, S. Hu, J. Li, D. Zhu, Z. Wang, J. Cores, K. Cheng, G. Liu, K. Huang, Extruded mesenchymal stem cell nanovesicles are equally potent to natural extracellular vesicles in cardiac repair, ACS Appl. Mater. Interfaces 13 (2021) 55767–55779, https://doi.org/10.1021/acsami.1c08044.

[17] T. Wang, W. Li, Y. Zhang, X. Xu, L. Qiang, W. Miao, X. Yue, X. Jiao, X. Zhou, Z. Ma, S. Li, M. Ding, J. Zhu, C. Yang, H. Wang, T. Li, X. Sun, J. Wang, Bioprinted constructs that simulate nerve-bone crosstalk to improve microenvironment for bone repair, Bioact. Mater. 27 (2023) 377–393, https://doi.org/10.1016/j.bioactmat.2023.02.013.

[18] R. Kalluri, V.S. LeBleu, The biology, function, and biomedical applications of exosomes, Science 367 (2020), https://doi.org/10.1126/science.aau6977.

[19] K.D. Popowski, P.C. Dinh, A. George, H. Lutz, K. Cheng, Exosome therapeutics for COVID-19 and respiratory viruses, View 2 (2021) 20200186, https://doi.org/10.1002/VIW.20200186.

[20] R.T. Miceli, T.Y. Chen, Y. Nose, S. Tichkule, B. Brown, J.F. Fullard, M.D. Saulsbury, S.O. Heyliger, S. Gnjatic, N. Kyprianou, C. Cordon-Cardo, S. Sahoo, E. Taioli, P. Roussos, G. Stolovitzky, E. Gonzalez-Kozlova, N. Dogra, Extracellular vesicles, RNA sequencing, and bioinformatic analyses: challenges, solutions, and recommendations, J. Extracell. Vesicles 13 (2024) e70005, https://doi.org/10.1002/jev2.70005.

[21] D. Zhu, S. Liu, K. Huang, Z. Wang, S. Hu, J. Li, Z. Li, K. Cheng, Intrapericardial exosome therapy dampens cardiac injury via activating Foxo3, Circ. Res. 131 (2022) e135–e150, https://doi.org/10.1161/CIRCRESAHA.122.321384.

[22] H. Zhuo, Y. Chen, G. Zhao, Advances in application of hypoxia-preconditioned mesenchymal stem cell-derived exosomes, Front. Cell Dev. Biol. 12 (2024) 1446050, https://doi.org/10.3389/fcell.2024.1446050.

[23] R. Toghiani, V. Azimian Zavareh, H. Najafi, M. Mirian, N. Azarpira, S.S. Abolmaali, J. Varshosaz, A.M. Tamaddon, Hypoxia-preconditioned WJ-MSC spheroid-derived exosomes delivering miR-210 for renal cell restoration in hypoxia-reoxygenation injury, Stem Cell Res. Ther. 15 (2024) 240, https://doi.org/10.1186/s13287-024-03845-7.

[24] K. Shen, A. Duan, J. Cheng, T. Yuan, J. Zhou, H. Song, Z. Chen, B. Wan, J. Liu, X. Zhang, Y. Zhang, R. Xie, F. Liu, W. Fan, Q. Zuo, Exosomes derived from hypoxia preconditioned mesenchymal stem cells laden in a silk hydrogel promote cartilage regeneration via the miR-205-5p/PTEN/AKT pathway, Acta Biomater. 143 (2022) 173–188, https://doi.org/10.1016/j.actbio.2022.02.026.

[25] T. Peng, M. Chai, Z. Chen, M. Wu, X. Li, F. Han, S. Chen, C. Liao, M. Yue, Y.Q. Song, H. Wu, L. Tian, G. An, Exosomes from hypoxia preconditioned muscle-derived stem cells enhance cell-free corpus cavernosa angiogenesis and reproductive function recovery, Adv. Healthc. Mater. 13 (2024) e2401406, https://doi.org/10.1002/adhm.202401406.

[26] M. Zhai, Y. Zhu, M. Yang, C. Mao, Human mesenchymal stem cell derived exosomes enhance cell-free bone regeneration by altering their miRNAs profiles, Adv. Sci. 7 (2020) 2001334, https://doi.org/10.1002/advs.202001334.

[27] K.Y. Cha, W. Cho, S. Park, J. Ahn, H. Park, I. Baek, M. Lee, S. Lee, Y. Arai, S.H. Lee, Generation of bioactive MSC-EVs for bone tissue regeneration by tauroursodeoxycholic acid treatment, J. Control. Release 354 (2023) 45–56, https://doi.org/10.1016/j.jconrel.2022.12.053.

[28] Y.K. Zhou, C.S. Han, Z.L. Zhu, P. Chen, Y.M. Wang, S. Lin, L.J. Chen, Z.M. Zhuang, Y.H. Zhou, R.L. Yang, M2 exosomes modified by hydrogen sulfide promoted bone regeneration by moesin mediated endocytosis, Bioact. Mater. 31 (2024) 192–205, https://doi.org/10.1016/j.bioactmat.2023.08.006.

[29] W.T. Yu, X.X. Su, M.X. Li, W.T. Wan, A. Li, H. Zhou, F. Xu, Three-dimensional mechanical microenvironment enhanced osteogenic activity of mesenchymal stem cells-derived exosomes, Chem. Eng. J. 417 (2021), https://doi.org/10.1016/j.cej.2020.128040.

[30] D. Wu, X. Chang, J. Tian, L. Kang, Y. Wu, J. Liu, X. Wu, Y. Huang, B. Gao, H. Wang, G. Qiu, Z. Wu, Bone mesenchymal stem cells stimulation by magnetic nanoparticles and a static magnetic field: release of exosomal miR-1260a improves osteogenesis and angiogenesis, J. Nanobiotechnol. 19 (2021) 209, https://doi.org/10.1186/s12951-021-00958-6.

[31] M.A. Fernandez-Yague, S.A. Abbah, L. McNamara, D.I. Zeugolis, A. Pandit, M. J. Biggs, Biomimetic approaches in bone tissue engineering: integrating biological and physicomechanical strategies, Adv. Drug Deliv. Rev. 84 (2015) 1–29, https://doi.org/10.1016/j.addr.2014.09.005.

[32] S.H. Moon, Y.W. Cho, H.E. Shim, J.H. Choi, C.H. Jung, I.T. Hwang, S.W. Kang, Electrically stimulable indium tin oxide plate for long-term in vitro cardiomyocyte culture, Biomater. Res. 24 (2020) 10, https://doi.org/10.1186/s40824-020-00189-0.

[33] L. Dejob, B. Toury, S. Tadier, L. Grémillard, C. Gaillard, V. Salles, Electrospinning of in situ synthesized silica-based and calcium phosphate bioceramics for applications in bone tissue engineering: a review, Acta Biomater. 123 (2021) 123–153, https://doi.org/10.1016/j.actbio.2020.12.032.

[34] J. Salbach-Hirsch, S.A. Samsonov, V. Hintze, C. Hofbauer, A.K. Picke, M. Rauner, J. P. Gehrcke, S. Moeller, M. Schnabelrauch, D. Scharnweber, M.T. Pisabarro, L. C. Hofbauer, Structural and functional insights into sclerostin-glycosaminoglycan interactions in bone, Biomaterials 67 (2015) 335–345, https://doi.org/10.1016/j.biomaterials.2015.07.021.

[35] J. Salbach, S. Kliemt, M. Rauner, T.D. Rachner, C. Goettsch, S. Kalkhof, M. von Bergen, S. Möller, M. Schnabelrauch, V. Hintze, D. Scharnweber, L.C. Hofbauer, The effect of the degree of sulfation of glycosaminoglycans on osteoclast function and signaling pathways, Biomaterials 33 (2012) 8418–8429, https://doi.org/10.1016/j.biomaterials.2012.08.028.

[36] H.D. Kim, E.A. Lee, Y.H. An, S.L. Kim, S.S. Lee, S.J. Yu, H.L. Jang, K.T. Nam, S. G. Im, N.S. Hwang, Chondroitin sulfate-based biomineralizing surface hydrogels for bone tissue engineering, ACS Appl. Mater. Interfaces 9 (2017) 21639–21650, https://doi.org/10.1021/acsami.7b04114.

[37] L. Zhou, L. Fan, F.M. Zhang, Y. Jiang, M. Cai, C. Dai, Y.A. Luo, L.J. Tu, Z.N. Zhou, X.J. Li, C.Y. Ning, K. Zheng, A.R. Boccaccini, G.X. Tan, Hybrid gelatin/oxidized chondroitin sulfate hydrogels incorporating bioactive glass nanoparticles with enhanced mechanical properties, mineralization, and osteogenic differentiation, Bioact. Mater. 6 (2021) 890–904, https://doi.org/10.1016/j.bioactmat.2020.09.012.

[38] P.M. Sivakumar, A.A. Yetisgin, S.B. Sahin, E. Demir, S. Cetinel, Bone tissue engineering: anionic polysaccharides as promising scaffolds, Carbohydr. Polym. 283 (2022) 119142, https://doi.org/10.1016/j.carbpol.2022.119142.

[39] R. Hess, A. Jaeschke, H. Neubert, V. Hintze, S. Moeller, M. Schnabelrauch, H. P. Wiesmann, D.A. Hart, D. Scharnweber, Synergistic effect of defined artificial extracellular matrices and pulsed electric fields on osteogenic differentiation of human MSCs, Biomaterials 33 (2012) 8975–8985, https://doi.org/10.1016/j.biomaterials.2012.08.056.

[41] J. Deng, X. Wang, W. Zhang, L. Sun, X. Han, X. Tong, L. Yu, J. Ding, L. Yu, Y. Liu, Versatile hypoxic extracellular vesicles laden in an injectable and bioactive hydrogel for accelerated bone regeneration, Adv. Funct. Mater. 33 (2023), https://doi.org/10.1002/adfm.202211664.

[42] L. Wang, Y. Pang, Y. Tang, X. Wang, D. Zhang, X. Zhang, Y. Yu, X. Yang, Q. Cai, A biomimetic piezoelectric scaffold with sustained Mg(2+) release promotes neurogenic and angiogenic differentiation for enhanced bone regeneration, Bioact. Mater. 25 (2023) 399–414, https://doi.org/10.1016/j.bioactmat.2022.11.004.

[43] F. Wang, S. Li, L. Kong, K. Feng, R. Zuo, H. Zhang, Y. Yu, K. Zhang, Y. Cao, Y. Chai, Q. Kang, J. Xu, Tensile stress-activated and exosome-transferred YAP/TAZ-Notch circuit specifies type H endothelial cell for segmental bone regeneration, Adv. Sci. 11 (2024) e2309133, https://doi.org/10.1002/advs.202309133.

[44] J. Yang, X. Gong, T. Li, Z. Xia, R. He, X. Song, X. Wang, J. Wu, J. Chen, F. Wang, R. Xiong, Y. Lin, G. Chen, L. Yang, K. Cai, Tantalum particles promote M2 macrophage polarization and regulate local bone metabolism via macrophage-derived exosomes influencing the fates of BMSCs, Adv. Healthc. Mater. 13 (2024) e2303814, https://doi.org/10.1002/adhm.202303814.

[45] L. Yu, G. Dou, H. Kuang, L. Bao, H. Liu, Q. Ye, Z. Wang, X. Yang, L. Ren, Z. Li, H. Liu, B. Li, S. Liu, S. Ge, S. Liu, Apoptotic extracellular vesicles induced endothelial cell-mediated autologous stem cell recruitment dominates allogeneic stem cell therapeutic mechanism for bone repair, ACS Nano 18 (2024) 8718–8732, https://doi.org/10.1021/acsnano.3c11050.

[46] S. Qie, N. Sang, Stanniocalcin 2 (STC2): a universal tumour biomarker and a potential therapeutical target, J. Exp. Clin. Cancer Res. 41 (2022) 161, https://doi.org/10.1186/s13046-022-02370-w.

[47] D.A. Jellinek, A.C. Chang, M.R. Larsen, X. Wang, P.J. Robinson, R.R. Reddel, Stanniocalcin 1 and 2 are secreted as phosphoproteins from human fibrosarcoma cells, Biochem. J. 350 (Pt 2) (2000) 453–461.